This article has been accepted for publication in a future issue of this journal, but has not been fully edited. Content may change prior to final publication. Citation information: DOI 10.1109/JLT.2018.2797104, Journal of Lightwave Technology

A Fabry–Perot interferometer strain sensor based on concave-core photonic crystal fiber

Jiajun Tian, *Member, IEEE*, Yuzhu Jiao, Qi Fu, Shaobo Ji, Zhigang Li, Mingran Quan, and Yong Yao

***Abstract*—A high-sensitivity Fabry–Perot interferometer (FPI) strain sensor based on a concave-core photonic crystal fiber (CPCF) was proposed and demonstrated. The FPI was formed by directly splicing a CPCF to a standard single-mode fiber. The CPCF was fabricated by cleaving a high-numerical-aperture solid-core photonic crystal fiber under axial tension using a traditional fiber cleaver. An FPI strain sensor with a cavity length of 4.85 μm and a strain sensitivity of 31.58 pm/με was successfully produced. The sensor also demonstrated a low temperature sensitivity of 0.653 pm/℃, reducing the cross-sensitivity between tensile strain and temperature. The benefits of the proposed sensor include simple fabrication, high strain sensitivity, and low temperature cross-sensitivity, making it attractive for practical applications.**

***Index Terms*—Fabry-Perot interferometer, concave-core photonic crystal fiber, fiber sensor.**

I. INTRODUCTION

WITH advantages including small size, light weight, corrosion resistance, and immunity to electromagnetic interference, fiber-optic strain sensors have been widely used for measuring strain in practical applications. They generally fall into the following categories, such as Fabry–Perot interferometer (FPI) fiber sensor [1], fiber Bragg grating (FBG) sensor [2-4], polarization type fiber sensor [5], Mach–Zehnder interferometer fiber sensor [6], and Sagnac interferometric configuration [7, 8]. Among these sensors, FPI fiber sensor has the advantages of simple structure, high sensitivity and compact size. The most commonly used FPI strain sensors generally comprise an in-line FPI structure with an air cavity in the fiber. This cavity is sometimes a micro notch in the fiber core fabricated through femtosecond laser micromachining [9-11]. However, this incurs high fabrication cost and produces a sensor with low mechanical strength. An alternative approach involves splicing a short section of a microstructure fiber, such as a hollow-core photonic crystal fiber (PCF) [12-14], and a capillary tube [15, 16] between two single-mode fibers (SMF) to form a typical sandwich structured FPI. This method has drawbacks of requiring multiple complex fabrication steps. It is also possible to form a microscopic air cavity inside the waveguide by splicing a solid-core PCF [17-22], capillary tube [16], or an SMF [23, 24] with an SMF using a standard arc-discharge technique. The main disadvantages of this approach are low reproducibility and minimal control over the cavity length. An air-cavity FPI strain sensor can also be fabricated using wet chemical etching [24-28]; however, unless a complex fabrication process is used, the corrosion depth cannot be effectively controlled. A high sensitivity FPI strain sensor also can be obtained by flame-brushing tapering technique assisted microfiber; however the fabrication of the microfiber is complex and has low reproducibility, and the mechanical strength of the fabricated sensor is low [29]. Moreover, both theoretical and experimental results show that the air-cavity-based FPI with a shorter cavity length has a higher strain sensitivity for the same structure and the same material [13, 16, 23, 30]. Therefore, the FPI with shorter cavity length and higher sensitivity has become a long-term goal for fiber FPI strain sensing. However, due to the fabrication technical limitations, very few FPIs have their lengths shorter than 10 μm [12-14, 16, 26]. Therefore, an approach for producing a fiber-optic air-cavity-based FPI strain sensor that offers simple fabrication, and high sensitivity is of great interests.

In this work, we demonstrate a promising technique for creating an air-cavity-based FPI wherein a concave-core PCF (CPCF) is spliced with a standard SMF. The CPCF is developed by cleaving a high-numerical-aperture solid-core PCF under axial tension, which provides a shallow concave core. After splicing the CPCF with the SMF, the concave core of the CPCF automatically forms an FPI cavity with a very short cavity length. The fabrication process is simple, requiring only few steps of cleaving and splicing. Such a short cavity length FPI can be used to produce a high-sensitivity strain sensor with a low cross-sensitivity to temperature. In particular, the proposed method was used to produce an FPI strain sensor with a cavity length of 4.85 μm and a sensitivity of 31.58 pm/με.

This work was financially supported in part by National Natural Science Foundation of China under Grants 61675055 and 61575051; in part by Shenzhen Municipal Science and Technology Plan Project under Grants JCYJ20150529114045265 and JSGG20150529153336124. *(Corresponding author: Jiajun Tian.)*

J. J. Tian, Y. Z. Jiao, Q. Fu, S. B. Ji, Z. G. Li, M. R. Quan, and Y. Yao are with the School of Electronic and Information Engineering, Shenzhen Graduate School, Harbin Institute of Technology, Shenzhen, Guangdong, 518055, China (e-mail: tianjiajun@hit.edu.cn; jiaoyuzhu@163.com; jxxyfq@126.com; jishaobo0424@163.com; lizhigang320@163.com; quanmingran@163.com; yaoyong@hit.edu.cn) .

Color versions of one or more of the figures in this paper are available online at http://ieeexplore.ieee.org. Copyright (c) 2015 IEEE.

0733-8724 (c) 2018 IEEE. Personal use is permitted, but republication/redistribution requires IEEE permission. See http://www.ieee.org/publications_standards/publications/rights/index.html for more information.

This article has been accepted for publication in a future issue of this journal, but has not been fully edited. Content may change prior to final publication. Citation information: DOI 10.1109/JLT.2018.2797104, Journal of Lightwave Technology

II. Fabrication and Working Principle

The fabrication process of the proposed FPI strain sensor is shown in Fig. 1. The CPCF is developed by cleaving a multimode solid-core PCF under axial tension. The multimode PCF (NKT MM-37-01, Blaze Photonics) has a high numerical aperture and a core diameter of 38 μm. It is surrounded by 20 large air holes with an azimuthal diameter of 12 μm and a radial

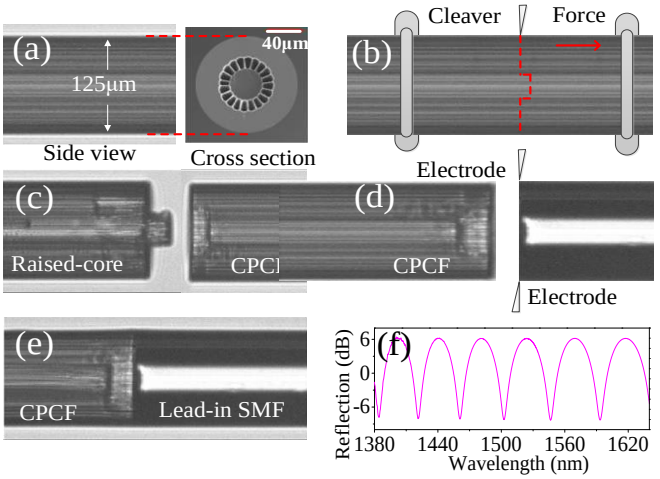

Fig. 1. Pictures of the in-line FPI strain sensor fabrication process under the fusion splicer. (a) The multimode PCF, side view (left) and cross-section (right); (b) The multimode PCF is cleaving by a cleaver under an axial tensile force; (c) Fabricated CPCF and raised-core PCF after cleaving multimode PCF; (d) splicing of CPCF with SMF with appropriate arc discharging position; (e) FPI fabricated using CPCF; and (f) Reflection spectrum of the fabricated FPI.

length of 24 μm [Fig. 1(a)]. These air holes are arranged close together so that the fiber core and the cladding are connected by 20 thin bridges each with a thickness of 3 μm. The outer diameter of the porous zone in the PCF cladding is about 86 μm. The cladding diameter of the multimode PCF is 125 μm, allowing it to be spliced with the standard SMF. The PCF was cleaved in a standard cleaver (Fujikura CT-30), under an axial tensile force applied by a weight through a pulley [not shown in Fig. 1(b)]. The 20 large air holes between the solid fiber core and the cladding converted the applied axial tension to a non-uniform axial strain between the fiber core and the cladding. This, in turn, produced an uneven radial fracture between the core and the cladding when the PCF was cleaved. The result is shown in Fig. 1(c). It can be seen that, after cleaving, a raised core was present at the left of the PCF, producing a concave core at the right. An FPI strain sensor was then fabricated by directly splicing a piece of the CPCF to a lead-in SMF (Corning SMF-28) using a fusion splicer (Fujikura FSM-80s). The splicer was set in CL-SM operation mode at an arc power of 40 bit and a duration of 100 ms. The CPCF was set 20 μm off the standard splicing point to avoid collapsing of the concave-core of CPCF during the splicing, as shown in Fig. 1(d). The lead-in SMF was used to guide the light to the sensor and collect the reflected light back to a spectrometer. Fig. 1(e) and (f) show a typical FPI sensor fabricated using this technique and its reflection spectrum, respectively. An air cavity can be clearly observed between the CPCF and SMF, formed directly by the concave core of the CPCF. The entire fabrication process required only few steps of cleaving and splicing using conventional splicer and cleaver, rendering the process simple and easy.

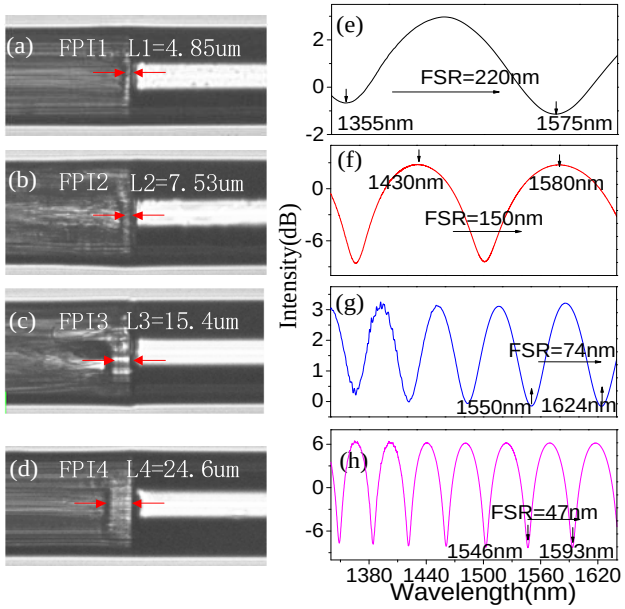

Fig. 2. (a), (b), (c), and (d): Fusion splicer images of the created FPI cavities with lengths of 4.85, 7.53, 15.4, and 24.6 μm, respectively; (e)–(h)The corresponding reflection spectra of the FPIs, respectively.

In the experiments we found that the length of the concave core of the CPCF was dependent upon the value of the axial tensile force. The full control over the length of the concave core could be achieved through adjustment of the tensile force by varying the weights used. Using this method, FPI strain sensors with different cavity lengths were fabricated by adjusting the weights used during PCF cleaving. The typical fabricated FPIs and their corresponding reflection spectra are shown in Fig. 2(a)–2(d) and Fig. 2(e)–2(h), respectively. Weights of 4, 6, 12, and 20 g were used in the experiments for FPI1~FPI4, respectively (the applied axial forces were calculated as 0.039, 0.059, 0.118 and 0.196 N, respectively). The interference patterns of the reflection spectra were clear, and the free spectrum range (FSR) decreased as the cavity length increased. It is also noticed that the fringe visibility in the interference spectrum is varied randomly from 3 dB to 14 dB for Fig. 2(e)–2(h). This may be caused by the inconsistent quality of the semi-mirror (end facet of the concave-core of CPCF) in the process of fiber cleaving with axial tensile force. However, due to the strain measurement of the FPI sensor is mainly based on tracking the wavelength shift of the fringes, the inconsistent fringe visibility of FPI has negligible impact on the strain measurement sensitivty. The follow-up experiments in this work demonstrated that even with the lowest fringe visibility, 3 dB, the FPI3 still can provide 12.53 pm/με strain sensitivity. The measured values of the FSR for the different FPI cavities were 220, 150, 74, and 47 nm, respectively, as shown in Fig. 2(e)–2(h). To calculate the cavity length, a low-finesse FPI model was used, which can be modeled using the two-beam optical interference equation [31]:

$$I_r = I_1 + I_2 + 2\sqrt{I_1 I_2}\cos\left(4\pi nL/\lambda + \phi_0\right) \qquad (1)$$

0733-8724 (c) 2018 IEEE. Personal use is permitted, but republication/redistribution requires IEEE permission. See http://www.ieee.org/publications_standards/publications/rights/index.html for more information.

This article has been accepted for publication in a future issue of this journal, but has not been fully edited. Content may change prior to final publication. Citation information: DOI 10.1109/JLT.2018.2797104, Journal of Lightwave Technology

where I_1 and I_2 are the intensities of the light reflected at the reflection faces; n and L are the refractive index and the length of the air cavity, respectively; ϕ_0 is the initial phase of the interference; and λ is the free space wavelength. From Eq. (1), the interference reaches a minimum when the phase of the cosine term becomes an odd number of π. The two adjacent interference minima have a phase difference of 2π. Therefore, the relationship between the wavelength spacing of two adjacent minima, or FSR, can be derived as follows [31]:

$$FSR = \lambda_1\lambda_2 / 2nL \quad (2)$$

From Eq. (2) and assuming the refractive index of air to be 1.0003, the known values of the FSR give cavity lengths of the fabricated sensors as 4.85, 7.53, 15.4, and 24.6 μm. The strain sensitivity of an FPI sensor is usually measured by tracking the shift in wavelength. When an external longitudinal force acts on the FPI sensor, the cavity length changes, and the corresponding longitudinal strain can be expressed by Eq. (3) [12]:

$$\varepsilon = F / SE \quad (3)$$

where ε, F, S, and E are the applied longitudinal strain, the applied longitudinal force, the cross-sectional area of the CPCF on the section of FPI cavity, and the Young's modulus of the fused silica (73 Gpa), respectively. From Eq. (3), the applied strain can be calculated by recording the longitudinal force applied.

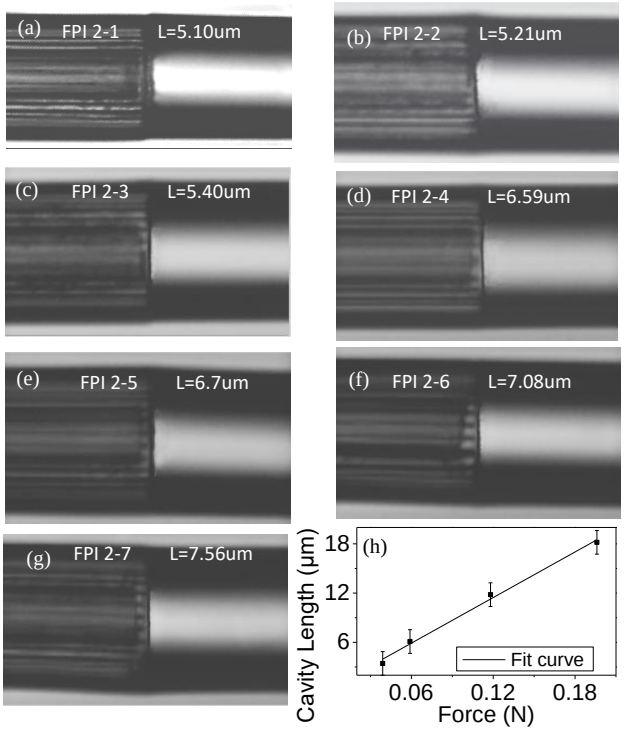

Fig. 3. (a)~(g)The microscopic photographs of fabricated FPIs with the axial tensile force of 6 g weights. (h) The relationship and error bar between the sensor cavity length and the applied tensile force.

In order to investigate the repeatability of the sensor fabrication, a large number of sensors were fabricated under the each tensile force condition. The relationship between the cavity length and the tensile force is shown in Fig. 3(h). For example, when the applied axial tensile force was fixed by using 6 g weights, seven CPCF-based FPIs were fabricated, and the cavity lengths were calculated by their interference spectra (not shown in Fig. 3) within a range from 5.1 to 7.56 μm, as shown in Fig. 3(a)~(g). The calculated cavity length is 6.44 μm with a standard deviation of 1.02 μm, or 15.8% of the cavity length.

III. Experimental Results and Discussion

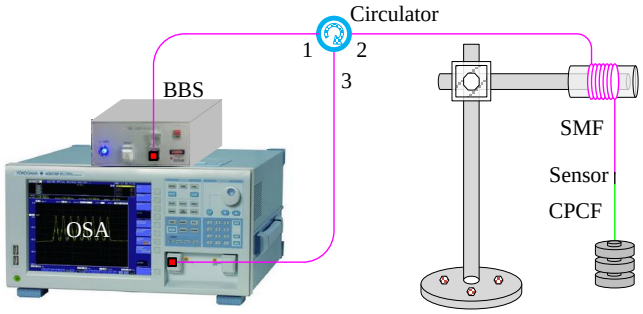

Fig. 4. The measured reflection spectra of FPI1–FPI4 as the applied force increased from 0 to 0.98 N in steps of 0.098 N.

Using this principle, we investigated the strain responses of CPCF-based FPI sensors with different cavity lengths. The experimental setup is shown in Fig. 4. It comprised a broadband light source (BBS, FiberLake ASE) with an output wavelength range from 1250 to 1650 nm, an optical circulator (OC), an optical spectrum analyzer (OSA, YOKOGAWA AQ6370C), and an optical support with a section of lead-in SMF twisted onto the arm. The BBS was connected to port1 of the OC to supply full-broadband light. The sensor was connected to port2 of the OC, and the weights were attached to the end of the CPCF. In order to facilitate the application of strain, a 0.5 m-long CPCF was retained for each sensor. The output reflection spectrum was recorded via OC port3 and measured by the OSA with a resolution of 0.02 nm.

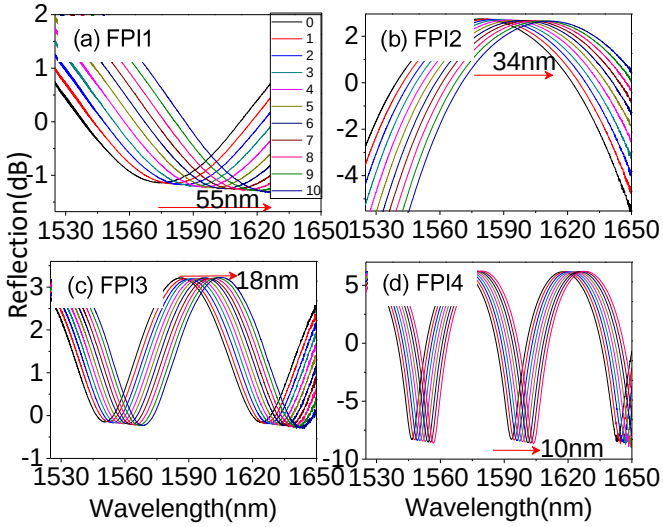

Fig. 5. The force response of sensors with different FP cavity lengths.

This experimental setup, shown in Fig. 4, was first used to measure the force response of the proposed sensor. The lead-in

0733-8724 (c) 2018 IEEE. Personal use is permitted, but republication/redistribution requires IEEE permission. See http://www.ieee.org/publications_standards/publications/rights/index.html for more information.

This article has been accepted for publication in a future issue of this journal, but has not been fully edited. Content may change prior to final publication. Citation information: DOI 10.1109/JLT.2018.2797104, Journal of Lightwave Technology

SMF of an FPI with a cavity length of 4.85 μm was fixed to the arm of the optical support, and a weight was attached to the CPCF. The number of weights (10 g each) was increased from 0 to 10, causing the applied longitudinal force to increase from 0 to 0.98 N in steps of 0.098 N. The wavelength shifts of the interference fringes around 1600 nm were measured as shown in Fig. 5(a). A linear shift toward longer wavelengths was observed as the weights were added. FPI strain sensors with cavity lengths of 7.53, 15.4, and 24.6 μm were applied to the measuring system, with the results shown in Fig. 5(b)–(d), respectively. The experimental results demonstrated that the cavity length had a significant effect on the shift in wavelength. As can be seen from Fig. 5(a)–(d), the range of the wavelength shift decreased from 55 to 10 nm as the cavity length of the FPI increased from 4.85 to 24.6 μm. This suggests that the longitudinal force sensitivity of an FPI sensor can be improved by decreasing the cavity length.

To investigate the longitudinal force sensitivity, the values of the peaks or dips at wavelengths around 1600 nm (Fig. 5) were derived using the second-order polynomial fitting method. The linear fitting results demonstrated that the proposed sensor had a good linear response to the tensile force, with force sensitivities of 52, 33, 21, and 13 nm/N at cavity lengths of 4.85, 7.53, 15.4, and 24.6 μm, respectively. Assuming the structure change of the CPCF can be ignored for the ideal splicing operation, the cross-sectional area of the FPI cavity was estimated to be 8317.156 μm^2 (the cross-sectional area of the fiber cladding plus the area of the 20 bridges subtracted from the cross-sectional area of the porous region). As the applied longitudinal force was known, the force-induced strain could be calculated by using Eq. (3). The results are shown in Fig. 6. Except for the fine linearity, the strain sensitivity was shown to increase significantly, from 8.05 to 31.58 pm/με, as the cavity length decreased from 24.6 to 4.85 μm. These experimental results agree well with those reported in earlier theoretical and experimental studies, which have proved that a shorter cavity length leads to a higher strain sensitivity [13, 15, 23]. It is noted that this method can produce an FPI with cavity length of only 4.85 μm, which is much shorter than that in previous studies [12-14, 16, 26], making it a promising candidate for high strain sensitivity measurement.

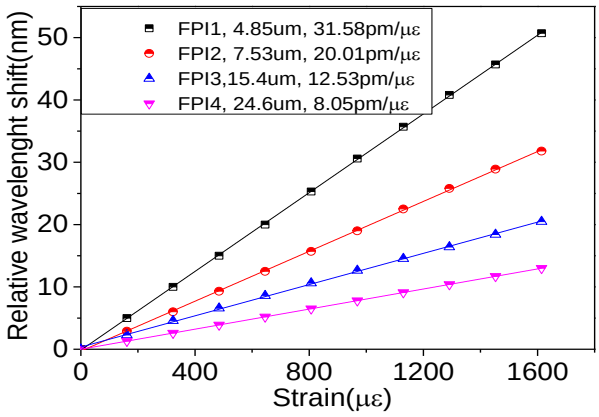

Fig. 6. Strain response for FPI of different cavity length

Meanwhile, in order to investigate the influence of the different wavelength dips in the interference spectrum on the sensor sensitivity, we measured the spectra of FPI4 under the different strain condition. A significant red shift of the spectrum was observed as the weights were added. The experimental results show that the dips at different wavelength have different strain sensitivity. Specifically, the dip with the longer wavelength has a higher sensitivity, as shown in Fig. 7. For example, the strain sensitivity is 7.39 pm/με for the dip at round 1460 nm. The strain sensitivity is increased to 8.07 pm/με for the dip at around 1600 nm. These experimental results are consistent with the results reported in [32]. Therefore, it is reasonable and appropriate to track the position of the dip or peak around the same wavelength of around 1600 nm of the different sensors, when we investigate the influence of the cavity length on the sensor strain sensitivity, as shown in Fig. 5.

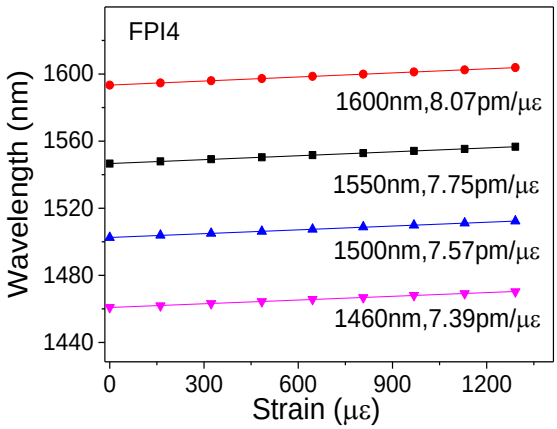

Fig. 7. The shift of different tracing wavelength versus strain.

In addition to allowing simple fabrication and providing high strain sensitivity, the proposed FPI sensor exhibited low temperature cross-sensitivity. An FPI strain sensor with a cavity length of 39.31 μm was tested. As the sensor fabrication involves the fusion splicing of the CPCF and the SMF, residual thermal stress may be induced in the process. Before measurement of the temperature response, the sensor was annealed in a furnace by gradually increasing the temperature from room temperature to ~200 ℃. The sensor was then placed in a high-temperature furnace (SIOM SG-XL1200). The reflection spectra at different temperatures were recorded by the OSA. In order to evaluate the temperature sensitivity of the proposed sensor, the wavelengths of the peaks in the spectra were found through curving fitting. Fig. 8 shows fringe valleys at wavelengths of about 1521.5 and 1551.5 nm. It can be seen that the fringe shifted slightly toward longer wavelength as the temperature rose. Using the linear fitting method, the temperature sensitivities of the fringes at wavelengths of 1521 and 1551.5 nm were calculated to be 0.653 and 0.598 pm/ ℃, which suggests a longer wavelength dip has higher temperature sensitivity. According to Eq. (3) in [12], we can obtain the relationship between the wavelength shift $\Delta\lambda$ and the temperature induced the refractive index change Δn and the cavity length change ΔL as below:

0733-8724 (c) 2018 IEEE. Personal use is permitted, but republication/redistribution requires IEEE permission. See http://www.ieee.org/publications_standards/publications/rights/index.html for more information.

This article has been accepted for publication in a future issue of this journal, but has not been fully edited. Content may change prior to final publication. Citation information: DOI 10.1109/JLT.2018.2797104, Journal of Lightwave Technology

$$\frac{\Delta\lambda}{\lambda}=\frac{\Delta n}{n}+\frac{\Delta L}{L}. \quad (4)$$

Due to the small thermo-optic coefficient of air, $2.85\times10^{-9}/℃$, the refractive index change of air cavity is quite small and can be ignored, when the environmental temperature changes. Meanwhile, due to the open cavity of the CPCF-based FPI, the influence of the air expansion on the cavity length can also be ignored. Therefore, the wavelength shift $\Delta\lambda$ induced by temperature change ΔT can be obtained as below:

$$\Delta\lambda=\lambda_0\times\frac{\partial L}{\partial T}\times\Delta T. \quad (5)$$

where $\frac{\partial L}{\partial T}$ is the thermal expansion coefficient of the silica ($5\times10^{-7}/℃$). As shown in Eq. (5), the temperature sensitivity is related to the indicator wavelength (λ_0). As a result, the fringes at longer wavelength have higher temperature sensitivity. At 1550 nm, the wavelength widely used for fiber-optic communication, the temperature sensitivity can be theoretically calculated as 0.775 pm/℃. As mentioned above, the temperature sensitivity obtained by the experimental test is 0.653 pm/℃, which agrees well with the theoretical result. The temperature-strain cross-sensitivity is calculated as 0.021 με/°C, which means for a temperature variation of 100 ℃, it only induces an error of 2.1 με. Therefore, temperature compensation is not required for most applications. If necessary, it can further reduce the temperature interference by the temperature compensation method with a fiber Bragg grating temperature sensor [33].

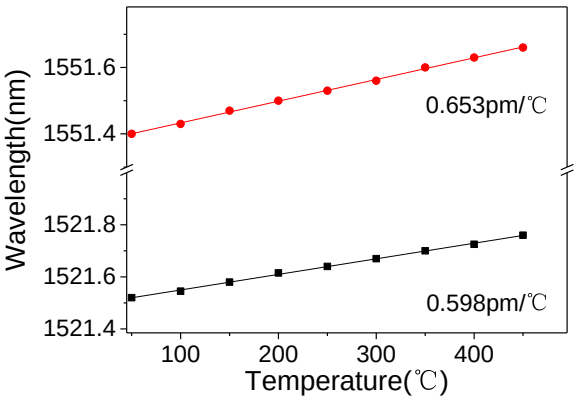

Fig. 8. The wavelength shift of different dips against temperature.

In order to make a proper performance assessment, we compared the proposed sensor with a few other FPI strain sensors reported in recent years, as shown in Table 1. It clearly suggests that, the proposed sensor here has the lowest temperature cross sensitivity and higher strain sensitivity than most of FPIs, which is attributed to the all-fiber open-cavity structure and the short cavity length. Although its strain sensitivity is lower than the micro-fiber based FPI [29] and the air bubble FPI [24], the proposed sensor has a more robust structure and lower temperature cross sensitivity.

To test the measurement repeatability of the proposed sensor, we conducted two separate measurements between 24 hours from 0 to 1614.1 με using a FPI with 6.68 μm cavity length. The experimental results show that the proposed sensor is repeatable, as illustrated in Fig. 9(a). The calculated average standard deviation for wavelength shift variations is less than

TABLE I
SOME AIR CAVITY FPI STRAIN SENSORS

Type	Cavity length (μm)	Sensitivity (pm/με)	Tep. Cro. Sen.(pm/℃)	References
F-P cavity machined by femtosecond laser	75 (PCF) 80 (SMF)	4.5 6	2 2.1	[9]
F-P: Hollow-core photonic	200	1.55	3	[12]
F-P: Hollow-core ring PCF	13	15.4	0.81	[13]
F-P: PCF + SMF	17	6.7	1	[17]
F-P: Hollow tube	17	13.9	27.5	[16]
F-P: Spheroidal cavity	58	2.7	1	[18]
F-P: microcavities	10	10.3	1	[19]
F-P: Hollow-core PCF	30	2.3	15	[20]
F-P: Suspended-core fiber	840	1.32	7.65	[21]
F-P: silica tube	17	13.9	1	[22]
F-P: rectangular air bubble	61	43	2	[24]
F-P:chemical etching	137	3.14	0.75	[28]
F-P:microfiber	21	200	1.98	[29]
F-P:Concave-core fiber	4.85	31.58	0.675	This work

0.72, and the strain sensitivity is stabilized at $19.635\pm0.174\ \mathrm{pm}/\mu\varepsilon$. The repeatability error is calculated to be 0.886%. We also tested the stability of the proposed sensor. The sensor has been continuously measured for 24 hours under the same strain condition. As shown in Fig. 9(b), the wavelength of the same dip in the spectrum of the sensor is stable. The calculated average standard deviation of the wavelength shift is small (1.08×10^{-4}) in the 24 hours measurement.

We also investigate the limit of detection (LOD) of the proposed sensor. As expressed in [34], the LOD of sensor is defined as below:

$$LOD=\frac{R}{Ss}, \quad (6)$$

where *Ss* is the sensor sensitivity. *R* is the sensor resolution, which characterizes the smallest possible spectral shift that can be accurately measured, and is affected by the spectral resolution and system noise. Considering that the fringe visibility of the sensor spectrum is related to the signal-to-noise ratio (SNR) and consequently has the effect on the LOD, we tested the spectral shifts of two typical sensors with different

0733-8724 (c) 2018 IEEE. Personal use is permitted, but republication/redistribution requires IEEE permission. See http://www.ieee.org/publications_standards/publications/rights/index.html for more information.

This article has been accepted for publication in a future issue of this journal, but has not been fully edited. Content may change prior to final publication. Citation information: DOI 10.1109/JLT.2018.2797104, Journal of Lightwave Technology

fringe visibilities, 2 dB and 8 dB, by continuously scanning the spectra for thirty times under the room temperature and the strain-free condition.

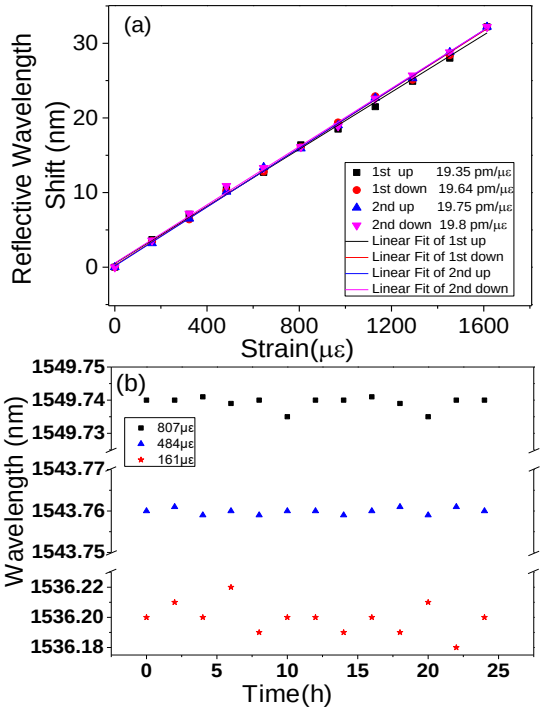

Fig. 9. (a) Wavelength shift of the proposed sensor versus different strain; (b) Long-time strain measurement of the proposed sensor.

The measured spectra for 2 dB and 8 dB sensors are shown in Fig. 10 (a) and (b), respectively [the detailed spectra around the fringe dip around 1532 and 1570 nm for tracking the wavelength shift are shown in the insets to Fig. 10 (a) and (b), respectively]. The values of the indicator dips were obtained by using the second-order polynomial fitting method, as shown in

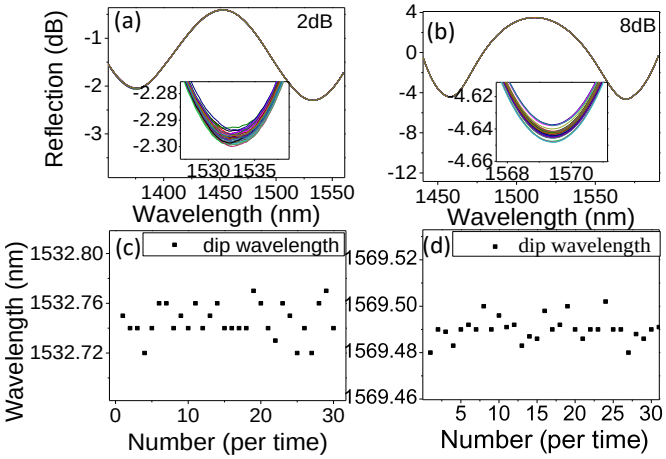

Fig. 10. Continuous 30 times spectral measurements for (a) 2 dB sensor and (b) 8 dB sensor; insets: enlarged views of the spectra around a fringe valley at 1530 nm and 1570 nm in (a) and (b), respectively; Spectral shifts in the continuous 30 times spectral measurements for (c) 2 dB sensor and (d) 8 dB sensor.

Fig. 10 (c) and (d), respectively. It is shown that the wavelength shift of the 2 dB sensor is ± 0.02 nm, while wavelength shift of 8 dB one is ± 0.01 nm. The experimental results are consistent with the theoretical analysis above, in which due to the higher SNR, the sensor with higher fringe visibility has a better sensor resolution. Taking Eq. (6) and sensor sensitivity of 31.58 pm/με, the LODs for 2 dB and 8 dB sensor are calculated as 1.26 and 0.63 με, respectively. Note that the LOD is also dependent upon the spectral resolution of measurement system. Thus, it can be further improved by using measurement equipment with a better spectral resolution than that we used in the present experimental setup.

IV. Conclusion

In summary, we proposed and demonstrated a novel technique for the fabrication of an air-cavity-based fiber-optic FPI. By adjusting the tensile force applied to the PCF during cleaving, the FPI cavity length could be controlled. An FPI with a cavity length as short as 4.85 μm was obtained. This in-fiber FPI sensor was then used to develop a high-sensitivity strain sensor. The strain sensor produced had a force sensitivity of 52 nm/N, a strain sensitivity of 31.58 pm/με, a temperature cross-sensitivity of less than 2.1×10^{-3} με/°C, and a limit of detection of 0.63 με. The fabrication process was simple. These advantages make the proposed sensor competitive in a wide range of practical applications.

References

[1] H. Xiao, J. Deng, G. Pickrell, R. G. May, and A. Wang, "Single-crystal sapphire fiber-based strain sensor for high-temperature applications," *J. Lightw. Technol.*, vol. 21 no. 10, pp. 2276-2283, 2003.

[2] C. Y. Lin, L. A. Wang and G. W. Chern, "Corrugated long-period fiber gratings as strain, torsion, and bending sensors," *J. Lightw. Technol.*, vol. 19 no. 8,pp. 1159-1168, 2001.

[3] S. Sulejmani, C. Sonnenfeld, T. Geernaert, G. Luyckx, D. V. Hemelrijck, P. Mergo, W. Urbanczyk, K. Chah, C. Caucheteur, P. Megret, H. Thienpont and F. Berghmans, "Shear stress sensing with bragg grating-based sensors in microstructured optical fibers," *Opt. Exp.*, vol. 21 no. 17, pp. 20404-20416, 2013.

[4] C. R. Dennison and P. M. Wild, "Superstructured fiber-optic contact force sensor with minimal cosensitivity to temperature and axial strain," *Appl. Opt*, vol. 51 no. 9, pp. 1188-1197, 2012.

[5] B. Hopf, A. W. Koch, and J. Roths, "Temperature dependence of glue-induced birefringence in surface-attached FBG strain sensors," *J. Lightw. Technol.*, vol. 34 no. 4, pp. 1220-1227, 2016.

[6] C. R. Liao, D. N. Wang, and Y. Wang, "Microfiber in-line mach-zehnder interferometer for strain sensing," *Opt. Lett.*, vol. 38 no. 5, pp. 757-759, 2013.

[7] J. Sadeghi, H. Latifi, J. L. Santos, Z. Chenari, F. Ziaee, "Behavior of a hollow core photonic crystal fiber under high radial pressure for downhole application," *Appl. Phys. Lett.*, vol.104 no.7, pp. 071910, 2014.

[8] J. Sadeghi, H. Latifi, M. Murawski, F. Mirkhosravi, T. Nasilowski, P. Mergo, K. Poturaj, "Group Polarimetric Pressure Sensitivity of an Elliptical-Core Side-Hole Fiber at Telecommunication Wavelengths," *IEEE J. Sel. Topics Quantum Electron*. vol. 22, no. 2, pp. 49-54, 2016.

[9] Y. J. Rao, M. Deng, D. W. Duan, X. C. Yang, T. Zhu, and G. H. Cheng, "Micro Fabry-Perot interferometers in silica fibers machined by femtosecond laser," *Opt. Exp.* , vol. 15 no. 21, pp. 14123–14128, 2007.

[10] Y. Gong, T. Zhao, Y. J. Rao, Y. Wu and Y. Guo, "A ray-transfer-matrix model for hybrid fiber fabry-perot sensor based on graded-index multimode fiber," *Opt. Exp.*, vol. 18 no. 15, pp. 15844-15852, 2010.

[11] J. Ma, J. Ju, L. Jin, W. Jin and D Wang, "Fiber-tip micro-cavity for temperature and transverse load sensing," *Opt. Exp.*, vol. 19 no. 13, pp. 12418-12426, 2011.

[12] Q. Shi, F. Lv, Z. Wang, L. Jin, J. J. Hu, Z. Y. Liu, G. Y. Kai, and X. Y. Dong, "Environmentally stable Fabry–Pérot-type strain sensor based on

0733-8724 (c) 2018 IEEE. Personal use is permitted, but republication/redistribution requires IEEE permission. See http://www.ieee.org/publications_standards/publications/rights/index.html for more information.

This article has been accepted for publication in a future issue of this journal, but has not been fully edited. Content may change prior to final publication. Citation information: DOI 10.1109/JLT.2018.2797104, Journal of Lightwave Technology

hollow-core photonic bandgap fiber," *IEEE. Photon. Technol. Lett.*, vol. 20 no. 4, pp. 237–239, 2008.

[13] M. S. Ferreira, J. Bierlich, J. Kobelke, K. Schuster, J. L. Santos, and O. Frazao, "Towards the control of highly sensitive Fabry-Pérot strain sensor based on hollow-core ring photonic crystal fiber," *Opt. Exp.*, vol. 20 no. 20, pp. 21946–21952, 2012.

[14] Y. J. Rao, T. Zhu, X. C. Yang, and D. W. Duan, "In-line fiber-optic etalon formed by hollow-core photonic crystal fiber," *Opt. Lett.*, vol. 32 no. 18, pp. 2662–2664, 2007.

[15] A. Zhou, B. Qin,Z. Zhu,Y. X. Zhang,Z. H. Liu,J. Yang,and L. B. Yuan, "Hybrid structured fiber-optic Fabry–Perot interferometer for simultaneous measurement of strain and temperature," *Opt. Lett.*, vol. 39 no. 38, pp. 5267–5270, 2014.

[16] M. S. Ferreira, P. Roriz, J. Bierlich, J. Kobelke, K. Wondraczek, C. Aichele, K. Schuster, J. L. Santos, and O. Frazao, "Fabry-Perot cavity based on silica tube for strain sensing at high temperatures," *Opt. Exp.*, vol. 23 no. 12, pp. 16063–16070, 2015.

[17] F. C. Favero, G. Bouwmans, V. Finazzi, J. Villatoro, and V. Pruneri, "Fabry–Perot interferometers built by photonic crystal fiber pressurization during fusion splicing," *Opt. Lett.* , vol. 36 no. 21, pp. 4191–4193, 2011.

[18] J. Villatoro, V. Finazzi, G. Coviello, and V. Pruneri, "Photonic-crystal-fiber-enabled micro-Fabry-Perot interferometer," *Opt. Lett.*, vol. 34 no. 16, pp. 2441–2443, 2009.

[19] F. C. Favero, L. Araujo, G. Bouwmans, V. Finazzi, J. Villatoro, and V. Pruneri, "Spheroidal Fabry-Perot microcavities in optical fibers for high-sensitivity sensing," *Opt. Exp.* Vol. 20 no. 7, pp. 7112–7118, 2012.

[20] S. H. Aref, R. Amezcua-Correa, J. P. Carvalho, O. Frazão, P. Caldas, J. L. Santos, F. M. Araújo, H. Latifi, F. Farahi, L. A. Ferreira, and J. C. Knight, "Modal interferometer based on hollow-core photonic crystal fiber for strain and temperature measurement," *Opt. Exp.* Vol. 17 no. 21, pp. 18669–18675, 2009.

[21] O. Frazão, S. H. Aref, J. M. Baptista, J. L. Santos, H. Latifi, F. Farahi, J. Kobelke, and K. Schuster, "Fabry–Pérot cavity based on a suspended-core fiber for strain and temperature measurement," *IEEE. Photon. Technol. Lett.* , vol. 21 no. 17, pp. 1229–1231, 2009.

[22] C. Aichele, J. Kobelke, J. L. Santos, J. Bierlich,M. S. Ferreira,P. Roriz,O. Frazao, K. Wondraczek, and K. Schuster, et al, "Measuring strain at extreme temperatures with a Fabry-Perot optical fiber sensor," *International Conference on Optical Fibre Sensors*, vol. 9634, pp. 96343P- 96343P-4, 2015.

[23] S. Liu, Y. P. Wang, C. R. Liao, G. J. Wang, Z. Y. Li, Q. Wang, J. T. Zhou, K. M. Yang, X. Y. Zhong, J. Zhao, and J. Tang "High-sensitivity strain sensor based on in-fiber improved Fabry–Perot interferometer." *Opt. Lett.*, vol. 39 no. 7, pp. 2121–2124, 2014.

[24] S. Liu, K. Yang, Y. Wang, J. Qu, C. Liao, J. He, Z. Li, G. Yin, B. Sun, J.Tang, and J. Zhao, "High-sensitivity strain sensor based on in-fiber rectangular air bubble," *Sci. Rep.*, 5, 7624, 2015.

[25] E. Cibula ,and D. Donlagic, "In-line short cavity Fabry-Perot strain sensor for quasi distributed measurement utilizing standard OTDR," *Opt. Exp.*, vol. 15 no. 14, pp. 8719–8730, 2007.

[26] V. R. Machavaram, R. A. Badcock, and G. F. Fernando, "Fabrication of intrinsic fiber Fabry–Perot sensors in silica fibers using hydrofluoric acid etching," *Sensor& Actuators A Physical*. vol. 138 no. 1, pp. 248–260, 2007.

[27] X. Chen, F. Shen, Z. Wang, Z. Huang ,and A. Wang, "Micro-air-gap based intrinsic fabry-perot interferometric fiber-optic sensor," *Appl. Opt*, vol. 45 no. 30 , pp. 7760-7766, 2006.

[28] P. A. R. Tafulo, P. A. S. Jorge, J. L. Santos and O. Frazão, "Fabry–pérot cavities based on chemical etching for high temperature and strain measurement," *Opt. Commun.*, vol. 285 no. 6,pp. 1159-1162, 2012.

[29] S. C. Gao ,W. G. Zhang, Z. Y. Bai, H. Zhang, W. Lin, L. Wang, and J. L. Li "Microfiber-enabled in-line Fabry–Pérot interferometer for high-sensitive force and refractive index sensing," *J. Lightw. Technol.*, vol. 32 no. 9, pp. 1682-1688, 2014.

[30] Y. Zhao, M. Q. Chen,R. Q. Lv, and F. Xia, "In-Fiber rectangular air fabry-perot strain sensor based on high-precision fiber cutting platform," *Opt. Commun.*, vol. 384, pp. 107-110, 2017.

[31] C. Wu, Z. Liu, A. P. Zhang, B. O. Guan, and H. Y. Tam, "In-line open-cavity Fabry-Pérot interferometer formed by C-shaped fiber for temperature-insensitive refractive index sensing," *Opt. Exp.*, vol. 22 no. 18, pp. 21757–21766, 2014.

[32] S. Gao, W. Zhang, Z. Y. Bai, H. Zhang, and W. Lin, "Microfiber-enabled in-line Fabry–Pérot interferometer for high-sensitive force and refractive index sensing." *J. Lightw. Technol.*, vol.32 no.9, pp. 1682-1688, 2014.

[33] J. Sadeghi, AH. Ghasemi, H. Latifi. "A label-free infrared opto-fluidic method for real-time determination of flow rate and concentration with temperature cross-sensitivity compensation." *Lab on a Chip*, vol.16 no.20, pp. 3957-3968, 2016.

[34] L. Gounaridis, P. Groumas, E. Schreuder, et al. "New set of design rules for resonant refractive index sensors enabled by FFT based processing of the measurement data." *Opt. Exp.*, vol. 24 no. 7, pp.7611-7632, 2016

Jiajun Tian received the Ph.D. degree from Harbin Institute of Technology, Harbin, China, in 2010. He is currently an Associate Professor with Harbin Institute of Technology, Shenzhen Graduate School. His current research interests include optical fiber sensors, and fiber lasers.

Yuzhu Jiao is currently working toward the M. S. degree at Harbin Institute of Technology, Shenzhen Graduate School, Shenzhen, China. Her current research interest is fiber sensors.

Qi Fu is currently working toward the M. S. degree at Harbin Institute of Technology, Shenzhen Graduate School, Shenzhen, China. His current research interests include fiber sensors and fiber lasers.

Shaobo Ji is currently working toward the M. S. degree at Harbin Institute of Technology, Shenzhen Graduate School, Shenzhen, China. His current research interests include fiber sensors and fiber-optic laser-ultrasound generation.

Zhigang Li is currently working toward the M. S. degree at Harbin Institute of Technology, Shenzhen Graduate School, Shenzhen, China. His current research interests include fiber sensors and fiber-optic laser-ultrasound generation.

Mingran Quan is currently working toward the M. S. degree at Harbin Institute of Technology, Shenzhen Graduate School, Shenzhen, China. His current research interests include fiber sensors and fiber lasers.

Yong Yao received the Ph.D. degree from South China Normal University, Guangzhou, China, in 2002. He is currently a Professor with Harbin Institute of Technology, Shenzhen Graduate School. His current research interests include optical fiber sensors, and fiber lasers.

0733-8724 (c) 2018 IEEE. Personal use is permitted, but republication/redistribution requires IEEE permission. See http://www.ieee.org/publications_standards/publications/rights/index.html for more information.